



Swansea University
Prifysgol Abertawe



Cronfa - Swansea University Open Access Repository

This is an author produced version of a paper published in :
Metallurgical and Materials Transactions B

Cronfa URL for this paper:

<http://cronfa.swan.ac.uk/Record/cronfa5829>

<http://dx.doi.org/10.1007/s11663-010-9410-4>

This article is brought to you by Swansea University. Any person downloading material is agreeing to abide by the terms of the repository licence. Authors are personally responsible for adhering to publisher restrictions or conditions. When uploading content they are required to comply with their publisher agreement and the SHERPA RoMEO database to judge whether or not it is copyright safe to add this version of the paper to this repository.

<http://www.swansea.ac.uk/iss/researchsupport/cronfa-support/>

**Microstructural characterisation of a polycrystalline nickel based superalloy
processed via TIG shaped metal deposition**

D Clark¹, MR Bache², MT Whittaker²

¹ Rolls-Royce plc, Elton Road, Derby, DE24 8BJ

² Swansea University, Singleton Park, Swansea SA2 8PP

Corresponding author: Dr M Whittaker, m.t.whittaker@swansea.ac.uk

+44 1792 295573 (Phone) +44 1792 295693 (Fax)

Abstract

Recent trials have produced tungsten-inert gas (TIG) welded structures of a suitable scale to allow an evaluation of the technique as an economic, commercial process for the manufacture of complex aero-engine components. The employment of TIG welding is shown to have specific advantages over alternative techniques based on metal inert gas (MIG) systems. Investigations utilising the nickel-based superalloy 718 have shown that TIG induces a smaller weld pool with less compositional segregation. In addition, since the TIG process involves a pulsed power source, a faster cooling rate is achieved, although this in turn compromises deposition rate. The microstructures produced by the two techniques differ significantly, with TIG showing an absence of the detrimental delta and laves phases typically produced by extended periods at high temperature using MIG. Instead, an anisotropic dendritic microstructure was evident with a preferred orientation relative to the axis of epitaxy. Niobium was found to be segregated to the interdendritic regions. Fine scale porosity was evident within the microstructure with a maximum diameter of approximately 5µm. This porosity was often found in clusters and usually associated with the

interdendritic regions. Subsequent post deposition heat treatment (PDHT) was shown to have no effect on pre-existing porosity and minimal effect on the microstructure.

Introduction

As part of ongoing trials assessing various techniques for their suitability to manufacture shaped metal deposited (SMD) structures, our latest efforts have concentrated upon tungsten inert gas (TIG) deposition. SMD typically involves increasing the thickness of material via localized, additive melting and solidification. The superposition of weld deposition beads is one technique that has received interest, largely due to the fact that the method can employ standard welding equipment. This latest research has benefited from a previous study using metal inert gas (MIG) since many of the processing techniques were shared ^[1]. One of the major conclusions from the previous work was that a smaller volumetric weld pool would be preferred; to provide a faster freezing rate and ultimately better microstructural control. This is a fundamental benefit of TIG, since the improved control of heat input at lower currents than those used for MIG can add to process stability for complex substrate forms. TIG also has a benefit in terms of precision of build. However, it is recognised that TIG offers a much slower deposition rate, which will limit the economic benefits of this technique. It is possible to electrically preheat the wire as employed in “hot wire TIG” to produce faster melt rates, although this has not been considered in this investigation. For simplicity a round wire consumable was used, not flattened to change lateral stiffness. In contrast, the lower deposition rate offers an advantage in terms of the rate of heat dissipation, allowing for a more consistent substrate temperature during the build up of the product form.

There are alternative economic factors in favour of TIG, including low capital equipment cost, especially when compared with competing wire based deposition techniques using wide spot lasers^[2] or electron beam guns. This is in addition to the efficient utilisation of consumable material, which is usually the main driver for additive techniques^[3]. In contrast to powder consumables, the use of wire as the feed supply for TIG provides a simple route to consistency and cleanliness of the source material. TIG lends itself to the use of finer feed wires which give a benefit in terms of current flux, again encouraging the relatively smaller melt pool, which in turn allows finer feature resolution. Any risk associated with a lack of fusion can be countered by the consistent delivery of the wire as opposed to powder fed to the hot zone of a weld pool, ultimately providing a more consistent microstructure within the deposit beads. In comparison with other arc-based techniques including the use of plasma, TIG is tolerant in terms of stand-off distance from the substrate through the addition of the filler wire which can act to regulate pool to contact tip distance providing power levels are kept in a stable range. TIG is also adaptable to various forms of process control (in terms of arc voltage, current and wire feed rate). Another benefit of the height tolerance compared to plasma processes is that TIG can readily be used to deposit structures on non-planar surfaces under automated control. Set against this are complexities of wire handling at corners, though powered wire feed retraction can often negate the need to adopt off-set co-axial wire feeding or the use of hockey stick shaped guide tubes.

In terms of the subsequent implications for structural integrity, TIG produces a relatively smooth surface finish to the deposited bead. Under certain circumstances

these TIG beads may not require subsequent machining in order to control surface finish within acceptance criteria, assuming the joint is not intended for service at a fatigue limiting location.

The combination of factors described above should offer TIG as a superior technique to MIG for the deposition of finer scaled, more complex features related to aero engine components. These could include mid-section engine components such as combustor casings, which require the addition of attachment locations in the form of flanges or non-axisymmetric boss features. Therefore, the present paper will detail a TIG-SMD structure fabricated from the nickel based superalloy IN718. This comprised a structure built up with 35 layers of weld beads. Detailed three-dimensional microstructural evaluations within individual beads are presented to highlight the different compositional phases present and any associated discrete, minor porosity. The implications for structural integrity are discussed in brief.

Experimental procedure

The TIG-SMD structure, Figure 1, was characterised in the as deposited condition. The control SMD parameters used to construct this sample are considered proprietary. These include control of arc energy levels^[4-6] and distribution together with the locus of acceptable wire position, orientation and attitude relative to the emergent deposited form. However, it can be confirmed that unlike the MIG structure reported previously^[1] the current material was deposited within an argon-filled enclosure. This would affect the energy distribution of the arc by changing the electron work function. Atmosphere affects the potential drop and hence the

associated arc constriction. Shielding gas will also affect surface heat transfer coefficients. In addition, the pulse rate on this occasion was significantly slower; the energy input reduced per unit length of deposition and the consumable feed rate was also reduced.

The through thickness dimension of the deposition beads was approximately 16 mm (i.e. transverse Y direction). Four metallographic specimens were extracted from the structure at the locations indicated in Figure 1. The whole structure was composed of approximately 35 layers of single-stringer width. Notably, one of the layers had a greater thickness, corresponding to a deliberate overnight interruption to the process which allowed the whole structure to cool to room temperature prior to re-commencing welding the following day. The arrows in Figure 1 highlight the location of this particular weld bead. It can be seen that specimens #1 and #3 sampled early depositions, while specimens #2 and #4 deliberately spanned the material deposited immediately before and after the interim shut down event.

Specimens were polished using standard metallographic techniques, and underwent a final chemical polish with an aqueous suspension of colloidal silica containing 20% H₂O₂ (hydrogen peroxide). At this stage specimens were inspected for evidence of porosity using a Reichart optical microscope equipped with a Nikon digital camera.

Subsequently, specimens were etched with a solution of 10ml HNO₃, 20ml HCl, 25ml distilled water and 10ml hydrogen peroxide (H₂O₂) for approximately 150 seconds. The response to etching was highly variable, even across the surface of

individual specimens. It was later evident that this variability was a trait of the underlying microstructure and not the preparation technique. Microstructural analysis was performed on both a Jeol 6100 SEM and Phillips XL30CP SEM. Chemical analyses were performed using a Jeol-35C SEM fitted with an Oxford Instruments EDX dispersion facility. Analysis was performed on all three orthogonal faces and the faces are defined using the axes superimposed on Figures 3-7.

Once the specimens had been analysed in the as received condition, they were heat treated in a high vacuum (10^{-6} mbar) furnace, according to the schedule detailed in Figure 2. This heat treatment cycle is based upon a typical sub-solvus procedure as discussed in a previous publication^[1] chosen to minimise the metallurgical effect on the parent substrate. The specimens were then re-polished, etched and re-examined.

During subsequent microstructural inspections, particular attention was paid to; the presence, location and distribution of delta or Laves phases, the form, size and shape of porosity found (if any) and any association with the microstructure, the orientation of microstructural features with respect to the homogeneity and axis of epitaxy.

Results

In terms of the microstructure a discontinuous phase was found to be concentrated in the interdendritic regions. The interdendritic region was identified through the use of EDX dispersion, which indicated a relatively high niobium content compared to the

matrix, consistent with previous publications^[7]. A typical example is shown in Figure 3. Small sub micron features were noted in the structure. These features were not associated with any discernable grain boundaries in the material. The structure was seen to be consistent within a single specimen, however, for consistency, similar areas were sampled across different specimens.

Two distinct morphologies of structure were noted on the X-Z plane, Figure 4. To the right hand side of this image an aligned interdendritically cored structure is evident. This linearly aligned dendrite structure relates to material solidification and growth. These aligned structures were generally orientated at an angle of approximately $\pm 30^\circ$ relative to the z direction (axis of deposition). The rate of solidification relation to process velocity has been described previously^[8]. Increasing the process velocity, U, increases the rate of heat dissipation from the pool, affecting pool volume. The curvature at the rear of the pool affects the ease of activation of grain nucleation and growth mechanisms, Figure 5. It can be seen that for nucleating grains, increasing pool concavity, as seen on the right of the cross section leads to a smaller encapsulated volume for the same nominal radius, with a greater degree of encasement in the parent heat sink. Similarly for the same cross sectional area of nucleate, there would be a greater average variance with radius from the instantaneous solidification surface normal along which a dendrite would find the greatest growth rate. Therefore, geometry of the pool as well as size would affect the kinetics of solidification as they affect homogeneous nucleation and growth^[9-11].

When viewed on the X-Y plane, any structural alignment of dendrites was absent, Figure 6. This plane, along the axis of processing, is close to being perpendicular to

the axis of epitaxy, crossing the primary dendrite cores. Clusters nucleating in the melt can only locate when growth conditions permit, turbulence and dendrite growth angles are expected to interact not only through changes in heat flux, but through rate of elemental replenishment and pressure on the growing dendrite tips.

It has also been previously reported^[12] that dendrites are affected by processing and that toolpath vector changes can affect epitaxial trends^[13]. Figure 7 indicates how the pitch of the heat source axis can create tracks with varying modes of energy density distribution. For a given interaction time, there is a minimum threshold of the three-dimensional energy distribution to fuse between layers. The modes of the energy intensity distributions affect the linearity of any interlayer features.

Examples of very fine porosity, often distributed in clusters, were noted throughout the microstructures. The pores, typically equi-axed in form, were intimately related to the interdendritic regions, which are the last to solidify, Figure 8. Individual pores were separated by less than 10 μ m, with the clusters typically separated by hundreds of microns.

Metallographic inspections within the beads immediately before and after the interim shutdown event showed that there was no effect on microstructure and in particular, there was no evidence of additional porosity. There was no evidence of centreline segregation associated with pool retention in the pulse regime.

A post deposition heat treatment was subsequently applied to the specimens under controlled vacuum conditions according to the routine defined in Figure 2. No change

in porosity distribution or size was noted due to this heat treatment, with no changes to the microstructures. Solidification structures were mainly unaffected, however, minor coarsening of the niobium rich coring was noted in some locations, Figure 9. Any aligned dendritic structures retained their original orientation.

Discussion

The present study has allowed a direct comparison between a TIG-based SMD process and previous trials conducted using MIG. For the 718 alloy at least, it is now considered that the heterogeneous MIG microstructures raise concerns over their potential impact on the high temperature creep performance. Different activation energies would apply throughout the different phases of this heterogeneous material [14-16]. There are also long slip paths available for dislocations generated in the material between the Laves/delta stringers^[17]. With creep strength being critical to nickel based alloys, particularly in gas turbine applications, unobstructed slip systems would be problematic. Dendrite cell size has also been linked to variations in dominant cracking mechanisms^[18]. It is noted that processing can optimise microstructural length scales. Furthermore, segregation distributions and interfacial energies resulting from thermal processing histories in the solidifying and precipitating regimes may affect modes of slip system suppression. As there were no significantly sized carbides visible in the MIG material to lock grain boundaries, then the creep life of this material may be expected to be sub-optimal. To counteract this, either the higher temperature cooling conditions governing carbide precipitation

kinetics could be controlled further, or an additional heat treatment processing stage cycle may need to be incorporated in such a process route.

TIG deposition is now considered worthy of further assessment in preference to MIG. The TIG process produced a smaller and more shallow weld pool size with a vertical heat sink as opposed to the side-wall heat sink produced under MIG with its associated high deposition rate conditions. The two processes differ greatly in terms of interpass conditions, with variations in time for the revisiting pass, the residual temperature of the deposit, the degree of remelting and the number of thermal excursions into precipitation temperature regimes for any given voxel. Obviously, varying any of these parameters will have an implication for the properties of the substrate, particularly in terms of microstructure.

The MIG employed a faster temporal pulse rate (i.e. frequency of high power input delivered over shorter time) which has an effect on solidification time and also gives a different pool shape, which has a direct effect on the heat sink characteristics of the deposit as well as the epitaxy and point of solidification, Figure 10^[19]. Changing pool penetration profile will also affect the surface area and hence the availability of grains with preferred growth angles. In the MIG process the epitaxy has a clear effect in that laves stringers lie along this direction, and their existence is a direct consequence of the prolonged and potentially cumulative exposure to high but subsolvus temperatures during cooling and repeat thermal excursions from adjacent deposition passes, together with chemical segregation, allowing such crystallographic changes as $\gamma'' \rightarrow \delta$ to occur, Figures 11 and 12. The presence of laves and δ phases are not unusual in cast microstructures and the size, form, location and morphology of the precipitation

response may be controlled for particular applications. This alloy is known to be used in a variety of microstructural conditions according to service application. Having elements locked in relatively large precipitates may be useful for opposing some modes of deformation. In addition, an associated depletion of niobium from the matrix would affect the sub-micron strengthening precipitation response.

In contrast, the initial microstructures produced by the TIG process are essentially encouraging. The microstructure contains a discontinuous coring of dendrite in the γ matrix, essentially in the form of a 3D grain structure. This is likely to give a more isotropic mechanical response. It is also worth considering that the response of the TIG material to non-destructive evaluation should be improved by the isotropy. The grain structure of the γ matrix should offer high strength due to a resistance to dislocation motion through the structure, and also avoids the brittle nature of the phases seen in the MIG structures. Whilst there is still evidence of some aligned dendrites within the TIG material, these are generally isolated, and do not have a common orientation, occupying any angle between $\pm 30^\circ$ with the axis of deposition. It is also possible that to improve creep properties in both MIG and TIG structures, consideration should be given to varying the programmed track of the heat source during the deposition process. The delta and laves precipitates seen in the MIG deposited structure were not seen in the TIG structure for the same nominal chemistry material with the same post deposition heat treatment cycle.

Of greatest concern in the MIG structure was the tendency to produce large-scale fissures, Figure 13. These fissures were consistently related to the Laves and delta phases, with cracking clearly evident along the direction of Laves stringers. In relation

to deposition processes, fissures such as these are a significant issue. However, individual smaller scale porosity also offers the possibility of fatigue crack initiation, by inevitably causing stress concentrations. Evidence of such porosity has been found in the TIG material, seen as fine interdendritic clusters lying along the axis of epitaxy. However, the fact that these clusters were isolated with distances between them being of the order of hundreds of microns means that the likelihood of crack coalescence is reduced. It is also worth noting that the porosity is generally spherical or near equiaxed, minimising the stress raising effect at least in terms of form. This porosity is different to that seen in the MIG process, where pores were often found approaching 100 μm in diameter and appeared to represent trapped gas.

As described earlier, the post deposition heat treatment given to the TIG structures had minimal effect on the microstructure, except for a slight coarsening of the cored regions. The interdendritic regions appeared to increase from a typical diameter of 3-4 μm to approximately 10-12 μm . It is useful to note that 3-4 μm was also typical of the diameter of Laves stringers in the MIG structures. This heat treatment cycle was chosen as a compromise, since supersolvus heat treatments are likely to cause distortion to the macro-structure and parent material. The deposition process caused a distortion to the substrate plate in Figure 1, however, in practise the substrate may comprise a constrained geometry or this effect could be compensated by in-process adjustment to the deposition rate (mass). This indicates a relatively high level of residual stress in the deposited material. These stress levels are inherent in the heat management approach for microstructure generation, as they relate to the thermal contraction of the deposited layer and re-melted volume against the substantially cooler, and therefore stronger, substrate. This substrate distorting effect can be

managed with technique and form geometry, but this was not a primary purpose of the present study. It was also recognised in a previous study that supersolvus temperatures were likely to be a major contributing factor to the detrimental phases seen in MIG structures^[1]. It is possible however, that employing a control of cooling rate may reduce this effect.

In-deposition process control of precipitation isotherms, together with information on transformation kinetics linked to finite element cells would be needed to predict and therefore optimise precipitate size and distribution density to a tighter degree. Greater process refinement may require combined and validated solidification^[20, 21], pool mixing^[22] and segregation^[21, 23]. It is noted that SMD operates in a dynamic system, modelling the rate of solid metal accumulation must take into account not only the change in pool temperature due to dilution by the sub-solidus consumable, but also the consequential change in arc stand-off which would change the energy distribution and hence thermo-capillary flow and pool profile and hence shaping of cooling isotherms. This wire to pool positional relationship must be considered in context of any considerations of specific energy per unit volume, i.e. voxel, as the bead cross section and hence heat flux distribution will vary with substrate geometry and cooling conditions.

Process interruptions and re-initiation may act as limiting factors to further refinement of precipitation density. If cooling rate can be controlled via appropriate tool path planning, timing, and heat extraction, as demonstrated by the potential of the TIG process interruption, then segregation could be limited such that the precipitation is

primarily governed by heat treatment. Heat extraction could be via techniques such as adaptively shaped conformal heat sinks or forced convective cooling.

The lower volumetric fill rate of the TIG process, relative to single or twin wire MIG, should mean the reaction time for standoff based control systems does not need to be so rapid, aiding the ability to control microstructure^[24]. Modern MIG systems with synergic controls are rapid, but these are typically based on simple geometry control curves or surfaces whereas SMD involves changing geometry and temperatures^[25]. It is noted that the processes are both scalable subject to the restrictions of physical and electromagnetic relationships, for example droplet deposition^[26] using 100 to 300 μm diameter filler wires. There will also be similarities with deposition using alternative heat sources^[27].

The cycle interruption and reinitiation changed the evolved substrate temperature and hence the heat sink for that stage in the process. This necessitated an adaptation in the parameters to ensure sufficient energy for fusion, wall width and wall profile. Changes in energy input distribution pattern and rate would affect the heat flux distribution, surface tension (seen in surface relief) and convective heat transfer, hence pool shape. There was no associated variation in segregation chemistry, or microstructure evident across this area.

The eventual microstructure will form during solidification and the post deposition heat treatment. Therefore pool shape and isotherm distribution will determine solidification vectors and freezing rates. The substrate temperature and shape will influence this pattern. Added to this are the consumable related effects of wire cross

section as the wire enters the pool, the wire shape, the feed rate and the direction, orientation, position and consistency of these wire pool entry variables. Arc constriction parameters are significant as the surface tension of the deposition pool influences the convective heat transfer patterns.

The oxidising potential of the melt surface also affects surface tension. Convective flow is especially significant in pulsed heat flux regimes as the influence on pool shape can affect the oscillation of the melt. In addition, the process travel speed, will affect the influence of the waveform, i.e. arc energy concentration, peak, background, pulse duration, over the distance of the bead, specifically the degree of axial overlapping. This will determine heat sink shape, and hence freezing behaviour and topographic contours, such as top surface ripples and side-wall undulations as illustrated in Figure 1.

The difference in microstructure appearance with plane of sectioning shows that there is still a tendency for vertical epitaxy despite the side-wall cooling of the elliptical cross-sectional shape of the pool. Deyev^[28] shows that the curvature of the surface on which nuclei form affects the degree of undercooling required, due to the work of nucleation for a stable nucleated volume. Pulses with deep pools also allow near full circumferential nucleation depending on overlapping rates and background heat flux. According to Gäumann^[20], this suggests a high rate of nucleation with vertically aligned columnar grains due to a low rear slope angle of the melt pool (i.e. less than 45° to the horizontal plane) and random rotational texture. The pulse repetition and volumetric overlap, together with the epitaxy from previous grains with different vertically epicentric axes of pool curvature, mean that there is no observable

correlation of grain boundary orientation or texture to process velocity. This could prove to be a useful method of randomising texture.

Conclusions

The following major conclusions have been drawn from the present research:

- TIG-SMD processed 718 materials have generated superior microstructures to previously employed metal inert gas (MIG) techniques ^[1]. Using the analysis techniques employed in this work, only niobium rich interdendritic regions were observed in TIG structures. Delta phase was regularly identified in MIG materials, along with the equally detrimental Laves phase. However, both were absent in the current TIG-SMD materials. This demonstrates the limited spatial and temporal exposure to excursions into the precipitation sensitive regime for the proprietary TIG processing regime.
- Very fine scale porosity was identified, associated with the interdendritic regions. No cracks or shrinkage fissures were noted although there was also fine interdendritic porosity.
- Processing with thermal management allows minimal δ formation and hence opens the potential for sub-solvus heat treatments for some applications, for example ageing treatments without prior homogenisation or solution treatments. This is of economic and practical benefit for hybrid-manufacturing process routes employing simplified wrought structures with additive features.

- Sub-solvus heat treatment had no effect on porosity and minimal effect on microstructure, with only a minor coarsening of niobium rich regions apparent.
- The microstructural condition of the TIG process compared with MIG leads to the conclusions that this technique deserves more consideration for structural applications.

Acknowledgements

The authors would like to thank Dr Steven Jones who developed the TIG SMD parameters, which were assessed, and Dr Paul Andrews, both of Rolls-Royce plc.

References

- [1] D. Clark, M.R. Bache and M.T. Whittaker: *Journal of Materials Processing Technology*, 203, 2008, pp 439–448.
- [2] C. Hung and J. Lin: *Journal of Laser Applications*, Volume 16, Issue 3, August 2004, pp 140-146.
- [3] K. Green., D. Clark: *RAPID* 2006, May 23, 2006.
- [4] R.W. Jnr. Messler: *Wiley-Interscience*, 1999.
- [5] P. Jiluan: *Woodhead Publishing, CRC Press*, 2003
- [6] J. Haidar: *Journal of Applied Physics*, 84, 1998, pp 3518-3529.
- [7] S.T. Wlodek and R.D. Field: *Superalloys 718, 625, 706 and Various Derivatives*, ed E.A. Loria, TMS 1994, pp 659-670.
- [8] W.F. Savage, *Weld World*, Vol 18, 1980, pp89-113

- [9] M. Rappaz, S.A. David, J.M. Vitek and L.A. Boatner: Metall. Trans. A, 21, pp1767-1782
- [10] W. Liu, J. DuPont: Acta Materialia, Vol. 52, Iss. 16, pp 4833-4847
- [11] S.A. David and J.M. Vitek: Int. Mater. Rev, 34, 1989, pp213-245.
- [12] S. Kou and L. Le,:Metall. Trans A, Vol.19, 1988, pp1075-1082
- [13] G.P. Dinda, A.K. Dasgupta, J. Mazumder: Materials Science and Engineering: A, Vol. 509, Iss. 1-2, 25 May 2009, pp 98-104
- [14] C.H. Caceres and J.R. Griffiths: Acta Materialia. Vol. 44, No. 1, 1996, pp 25-33.
- [15] Dye D.; Stone H.J.; Reed R.C.: Acta Materialia, Volume 49, No. 7, 2001, pp 1271-1283
- [16] Ş. Yilmaz and A. Aran: Materials Science and Technology, Vol. 14, No. 11, 1998, pp 1154-1162
- [17] F. Alexandre, S. Deyber, A. Pineau: Scripta Materialia, 50, 2004, pp 25-30.
- [18] C.H. Caceres, C.J. Davidson and J.R. Griffiths: Materials Science and Engineering A, 197 1995, pp 171-179.
- [19] E.E. Brown and Donald R. Muzyka, in book "Superalloys II, High Temperature Materials for Aerospace and Industrial Power", Edited by Chester T. Sims, Norman S. Stoloff, William C. Hagel, P182 (fig 8), Chapter 6 (Nickel-Iron Alloys)
- [20] M. Gäumann. C. Bezençon, P. Canalis and W. Kurz: Acta Materialia. 49 (2001) pp 1051-1062.
- [21] O. Hunsiker, D. Dye and R.C. Reed: Acta Materialia, Vol.48 No.17, 2000, pp 4191-4201

- [22] N. Chakraborty, S. Chakraborty and P. Dutta : Numerical Heat Transfer Part A, no. 45, 2004, pp 391-413.
- [23] N. Saunders: Superalloys 1996, eds R.D. Kissinger et al, (TMS, Warrendale) pp 101.
- [24] J.C. Lippold: Welding Journal, 73, 1995 (6), pp 129s-140s
- [25] P.W. Fuerschbach : in Trends in Welding Research, H. B. Smartt, J.A. Johnson and S.A. David, Eds, TMS, Warrentville, PA, pp 493-497, (5-8th June 1995), Gatlinburg, Tennessee .
- [26] N. D'Souza, M. Lekstrom, H.J. Dai, B.A. Shollock and H.B. Dong: Materials Science and technology, Vol 23, No 9, 2007, pp 1085-1092.
- [27] M. Terakubo, Janghwan Oh, S. Kirihara, Y. Miyamoto, K. Matsuura, M. Kudoh: Materials Science and Engineering A, 402, 2005, pp 84-91
- [28] G. Deyev, D. Deyev, "Surface Phenomena in Fusion welding Processes", Taylor & Francis, 2005

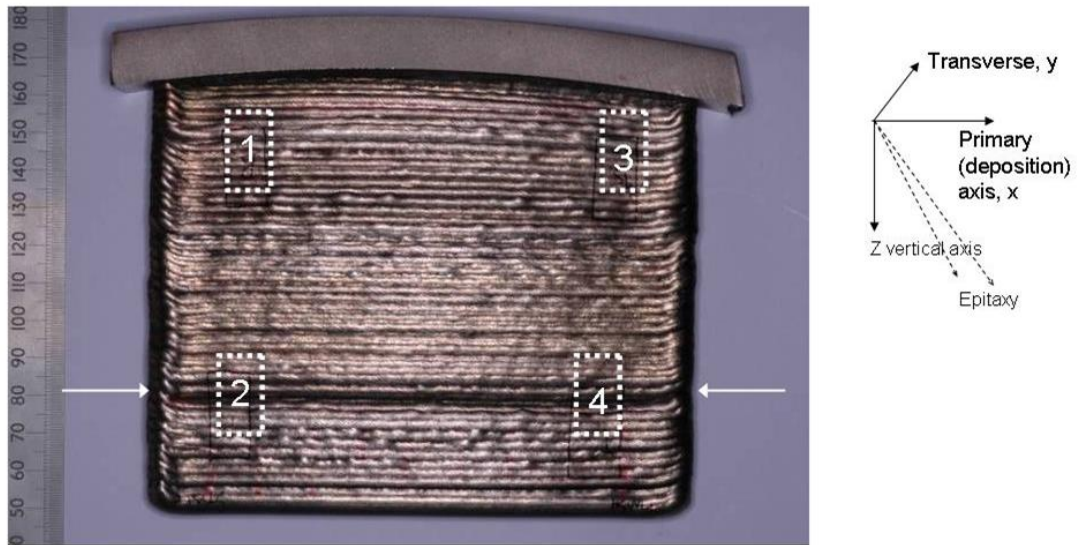


Figure 1: As processed TIG-SMD structure (shut down event marked by arrows).

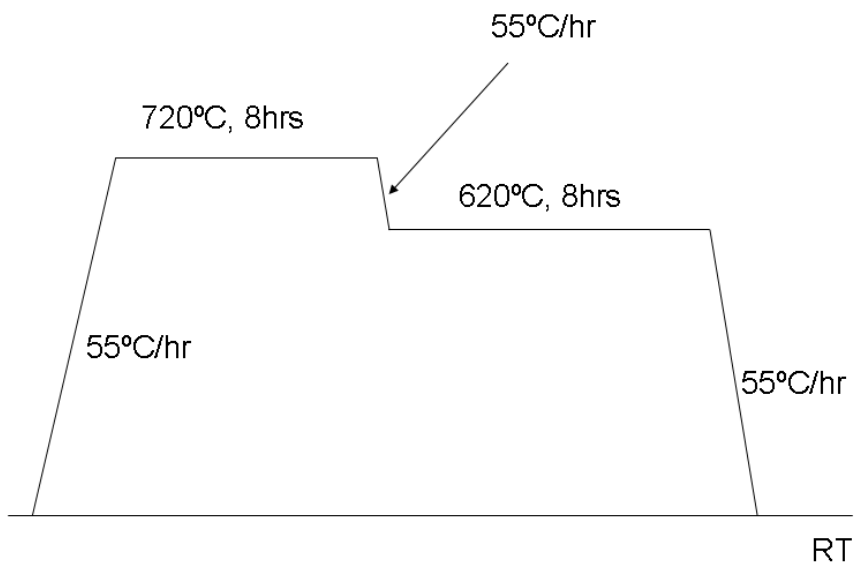


Figure 2: Post deposition heat treatment of TIG specimens.

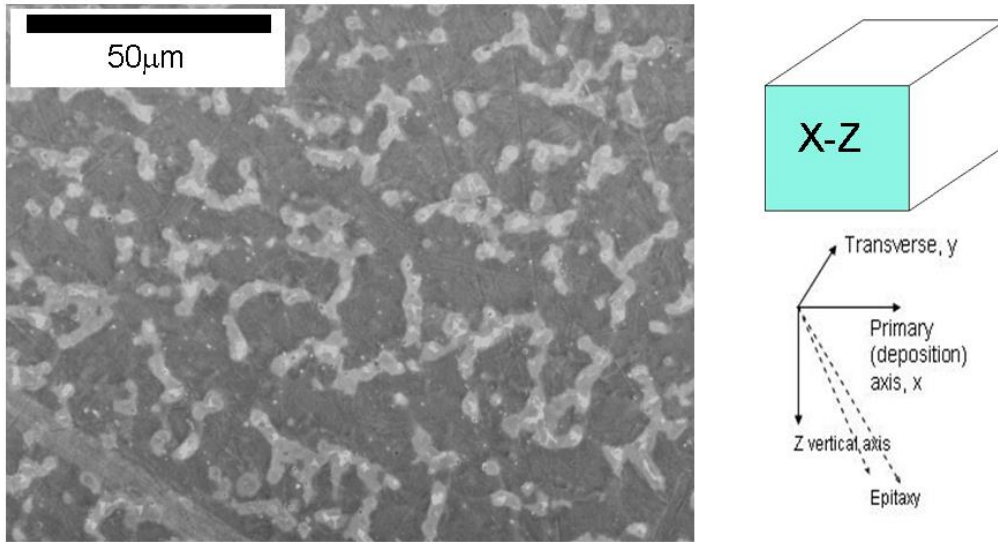


Figure 3: Niobium rich dendritic structure for TIG processed material, specimen #2, X-Z plane (as deposited).

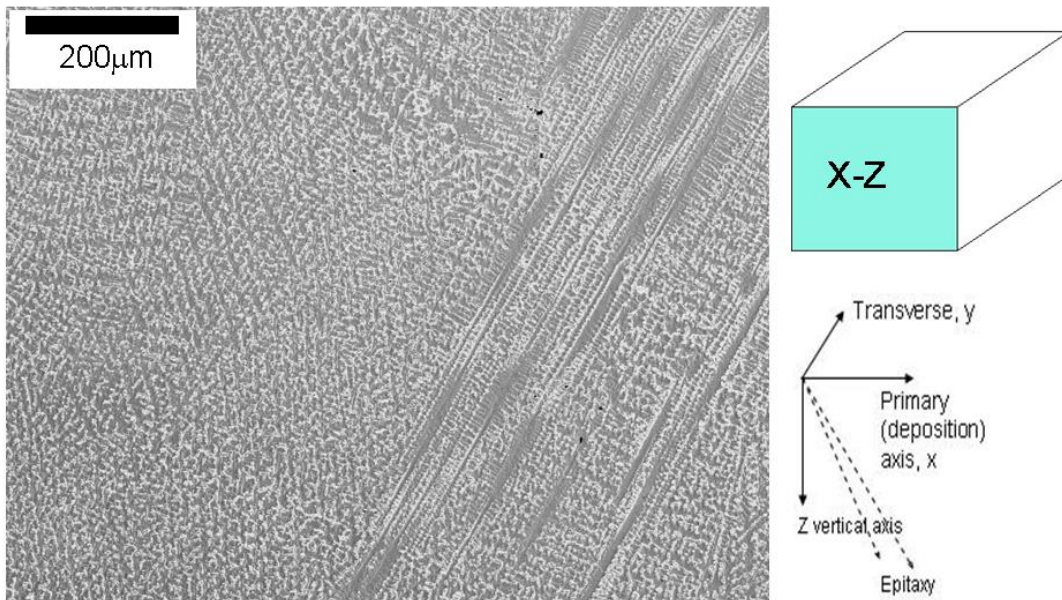


Figure 4: Dendrite structure for TIG processed material. Variation in dendrite core and branching orientations resulting from competitive grain growth from positions

around the melt pool. Of particular interest is the extent of the dendrite alignment of the segregation patterns (Specimen #1, X-Z plane, as deposited).

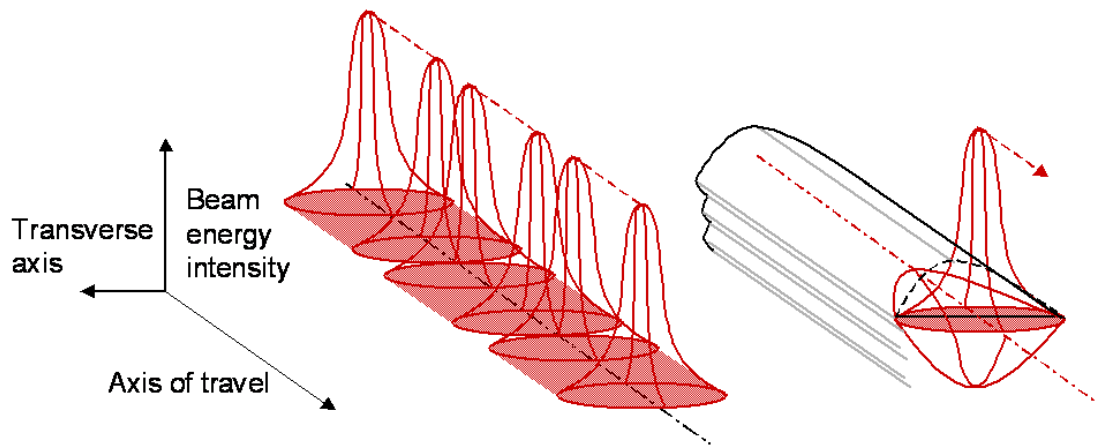


Figure 5: Schematic cross-section through discontinuously deposited material, indicating the instantaneous solidus isotherm, the gradient across which, together with the travel speed determines the development of aligned coring and grain size effects. Note that the actual pulse pitch regime was proprietary.

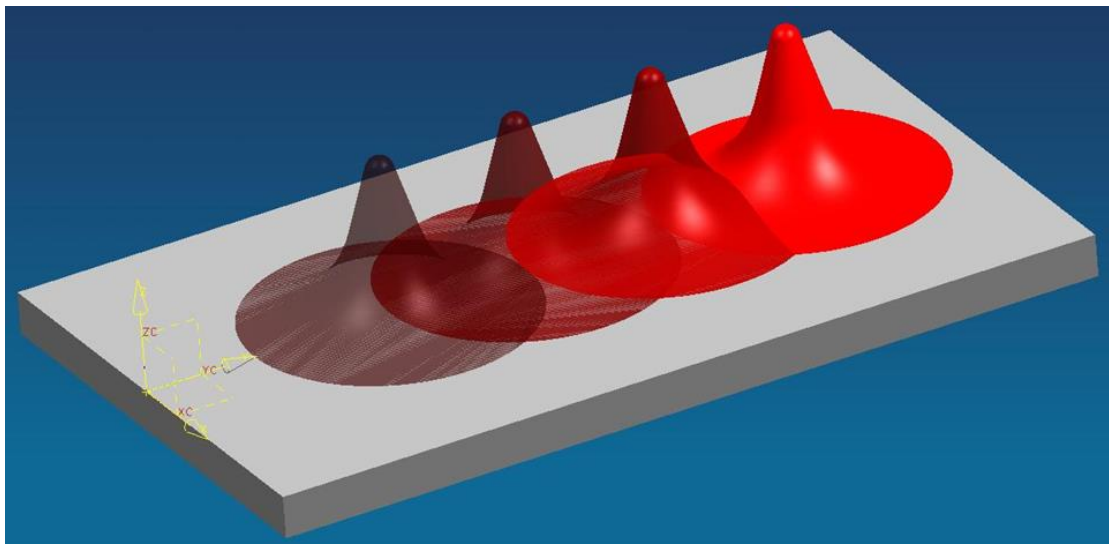


Figure 6: Effect of pulse pitch of the heat source axis on input energy density distribution. Note that the actual pulse pitch regime was proprietary

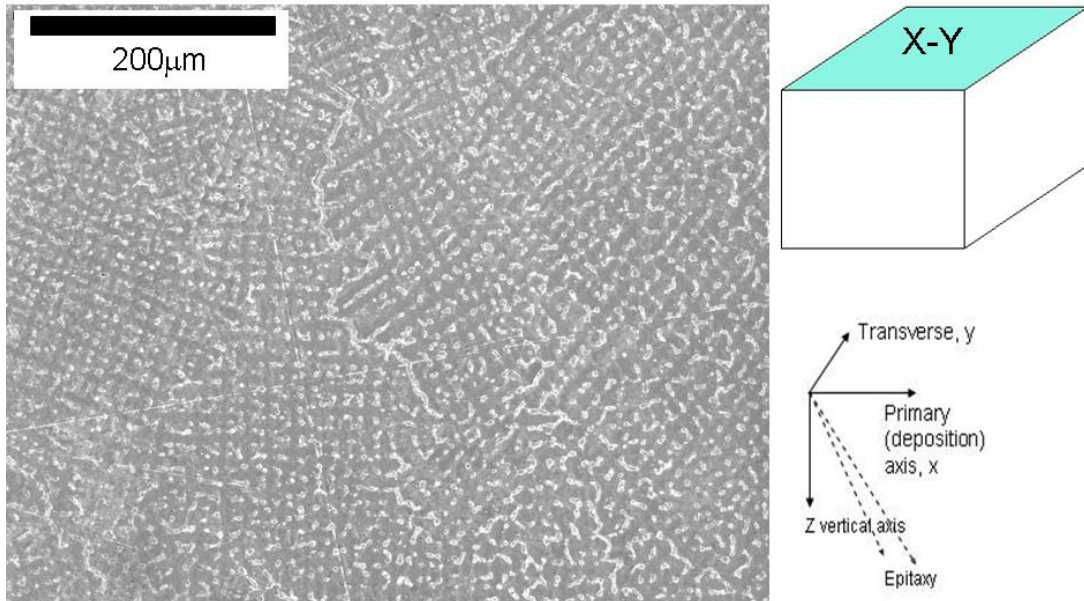


Figure 7: Absence of aligned dendrites across the X-Y plane of TIG processed material, Specimen #3, as-deposited.

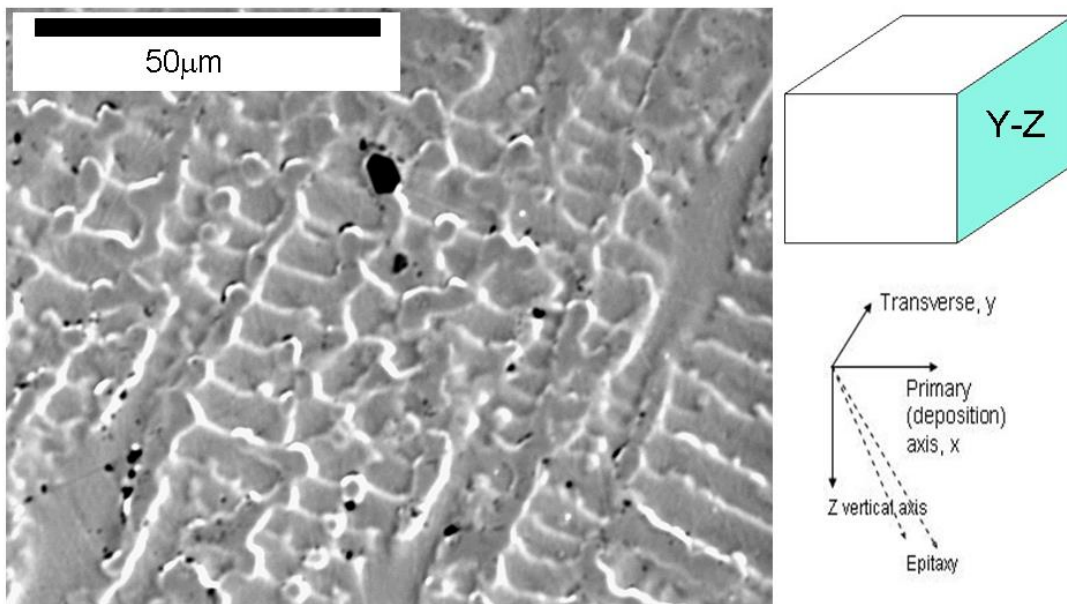


Figure 8: Discrete porosity, TIG processed material (Specimen #4, Y-Z plane, as deposited).

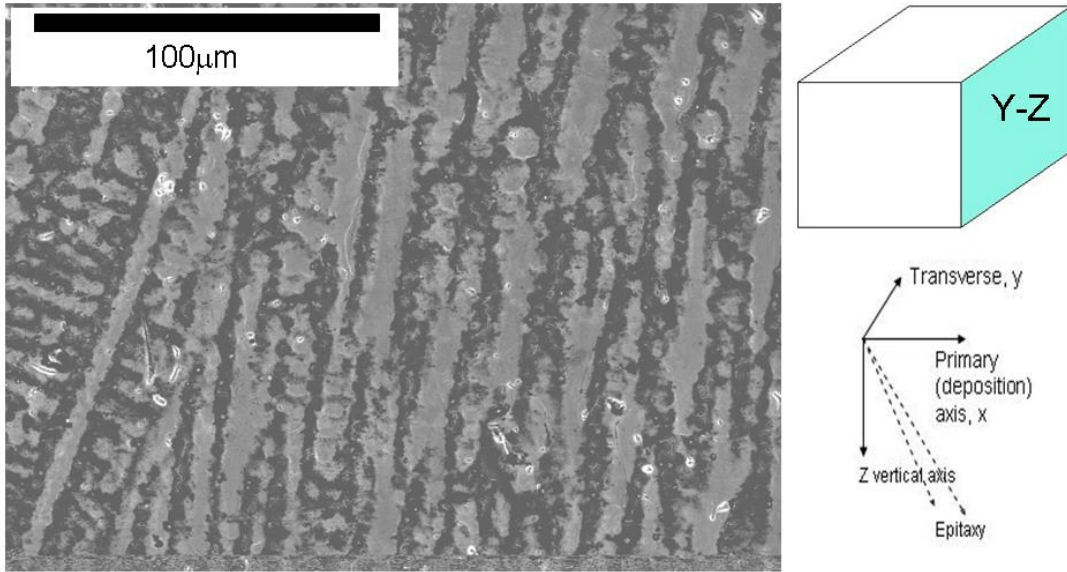


Figure 9: Coarsened interdendritic region after to heat treatment (Specimen #3, Y-Z plane, aged as shown in Figure 2)

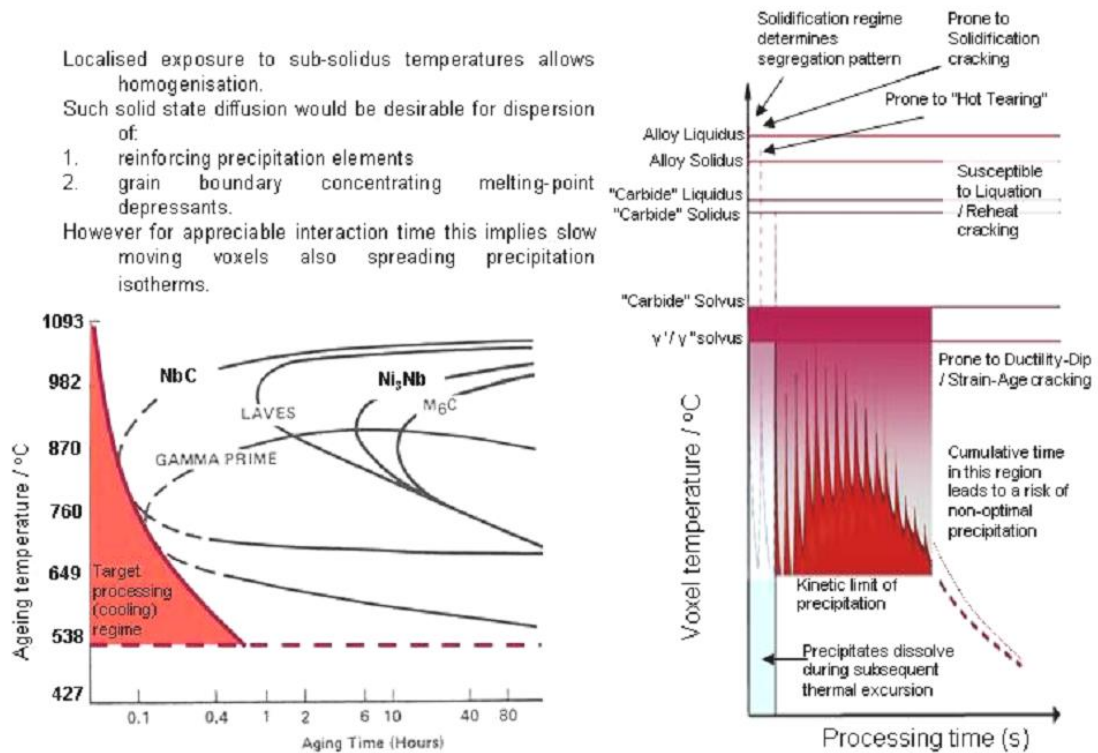
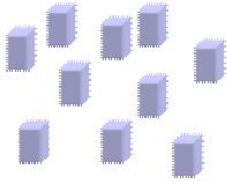


Figure 10 (a): Effect of temporal pulse rate and relation to thermal history for a specific volume of deposited material. Left diagram adapted from the literature for

isothermal behaviour of typically wrought 718 alloys [Sims, Chester T., Stoloff, Norman S., Hagel, William C. "Superalloys II", book, John Wiley & Sons, 1987].

A preferred texture tends towards directionally solidified properties



A quasi random texture tends towards isotropic properties.

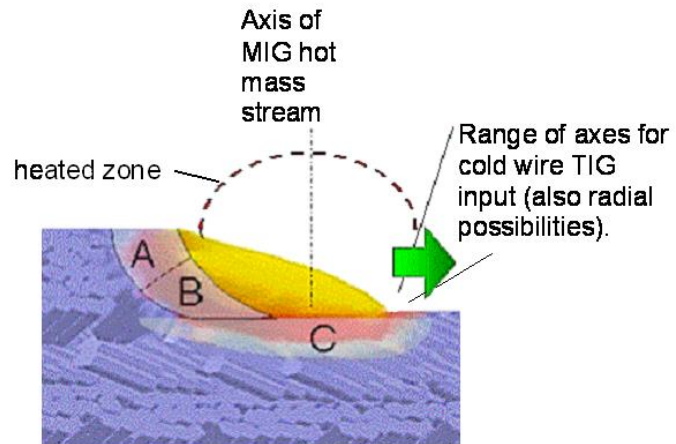
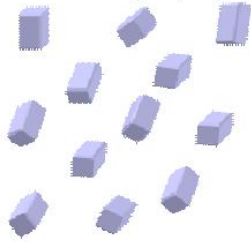


Figure 10 (b): Schematic side view of an arc-melted pool following a zig-zag (forward and reverse) toolpath. Grains grown along different growth axes according to position around the rear of the pool grains originating from zones A, B and C combine to create the material texture.

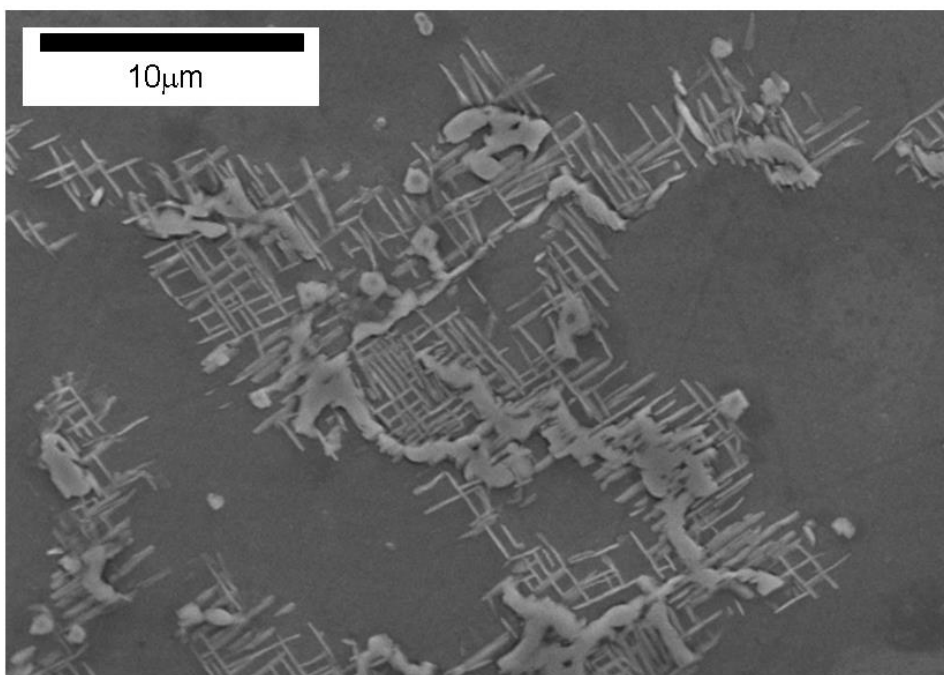


Figure 11: Laves & delta phase precipitates in MIG structures (aged as shown in Figure 2).

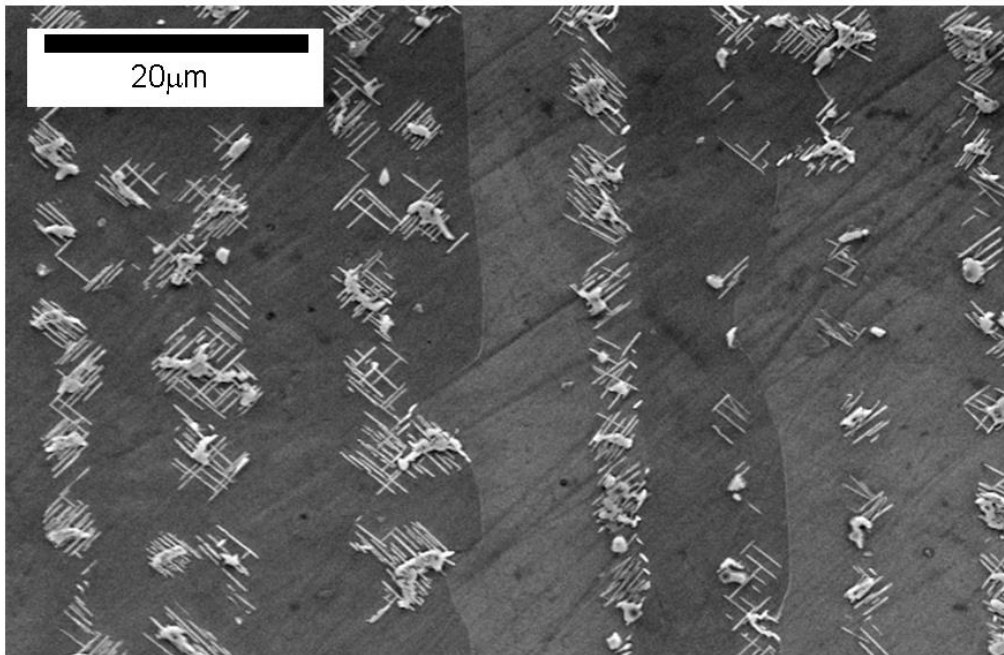


Figure 12: Laves & delta phases interdentritically aligned in MIG structure (aged as shown in Figure 2).

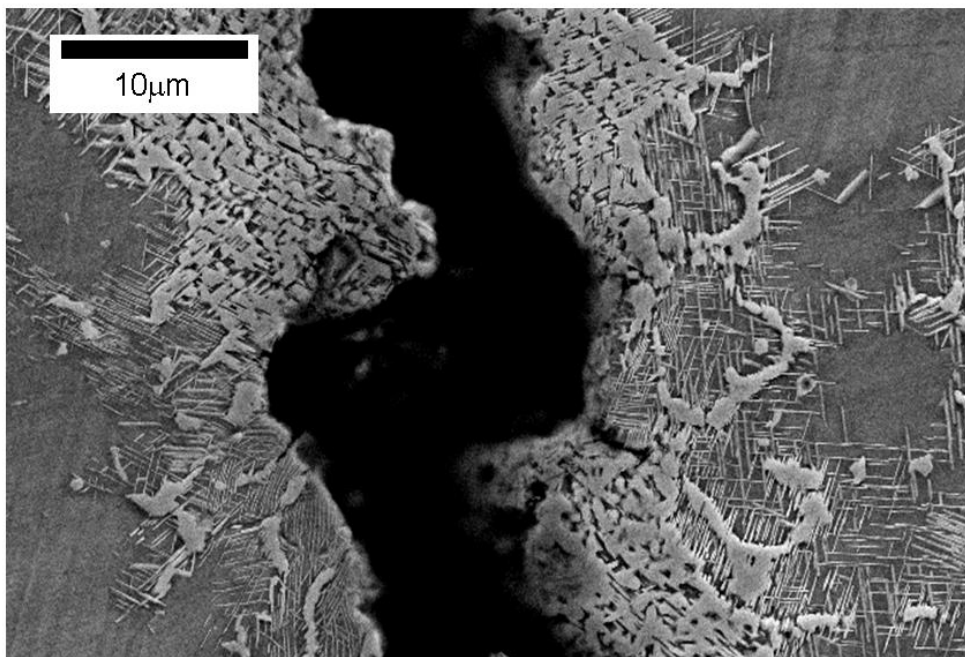


Figure 13: Large scale fissure surrounded by Laves & delta phase eutectics in MIG structure, aged as shown in Figure 2.